First-Principles Simulations of the Initial Phase of Self-Aggregation of a Cyanine Dye: Structure and Optical Spectra

Frank Haverkort, Anna Stradomska, and Jasper Knoester*

Zernike Institute for Advanced Materials, University of Groningen, Nijenborgh 4, 9747 AG Groningen, The Netherlands

E-mail: j.knoester@rug.nl,Tel:+31503634617

*To whom correspondence should be addressed

Abstract

Using first-principles simulations, we investigated the initial steps of the self-aggregation of the dye pseudoisocyanine (PIC) in water. First, we performed molecular dynamics (MD) simulations of the self-aggregation process, in which pile-of-coins oligomers ranging from dimers to stacks of about 20 molecules formed. The oligomer structures were found to be very flexible, with the dimers entering a weakly coupled state and then returning to a stable $\pi - \pi$ stacked conformation on a nanosecond timescale. The structural information from the MD simulations was combined with quantum chemical calculations to generate a time-dependent Frenkel exciton Hamiltonian for monomers, dimers, and trimers, which included vibronic coupling. This Hamiltonian, in turn, was used to calculate the absorption spectra for these systems. The simulated dimer spectrum compared well to experiment, validating the face-to-face stacked dimer arrangement found in our MD simulations. Comparison of the simulated trimer spectrum to experiment suggested that oligomers larger than the dimer cannot be abundant at the onset of J-aggregation. Finally, the conformation of the PIC J-aggregate was investigated by testing the stability of several possible conformations in our MD simulations; none of the tested structures was found to be stable.

Keywords: self-assembly, molecular aggregates, pseudoisocyanine, spectroscopy, Frenkel excitons, first-principles modeling

1 Introduction

The ordered structures that are formed by the self-aggregation of synthetic dye molecules have formed a flourishing area of research for decades.[1–4] These molecular aggregates have been used as sensitizers in traditional photography[5,6] and are promising building blocks for nanoscale functional materials, with applications such as light harvesting,[7,8] lasing[9,10] and materials with nonlinear optical functionality.[11–16] Also nature offers inspiration for self-aggregated functional systems: aggregates of dye molecules are used in photosynthesis by

plants and light-harvesting bacteria to absorb sunlight and transport the resulting excitation energy to the photosynthetic reaction center.[17–19] In addition, molecular aggregates give rise to unexpected collective phenomena that are interesting from a fundamental viewpoint. Despite the continuing effort focused on molecular aggregates and the successes of phenomenological modeling, many questions remain unanswered, not only about the optical and energy transport properties of the aggregates themselves but also on the way the aggregates are formed. Here, we will focus on the initial stages of self-aggregation, using as object of our study the cyanine dye 1,1'-diethyl-2,2'-cyanine (pseudoisocyanine, PIC, see Figure 1). This was the first molecule for which J-aggregation was discovered[1–4] and its aggregates are exemplary in the sense of yielding an exceptionally sharp J-band (i.e., an absorption band that is redshifted relative to the monomeric absorption spectrum).

In the past, several investigations of the initial steps of the aggregation process of PIC have been performed using spectroscopic techniques[20–23] (as well as examinations of similar dyes[24,25]). These investigations found that in the first stages of aggregation, several peaks appear on the blue side of the monomer absorption band, which are usually ascribed to dimers or larger oligomers with an H-aggregate character; as the aggregation progresses, a narrow and intense band appears on the red side of the monomer band, which is ascribed to the J-aggregate, and the other spectral bands decrease in intensity. It remained an open question how the transition from small oligomers with blueshifted absorption to large J-aggregates with redshifted absorption takes place. Also, there is as of yet no certainty on the molecular structure of the PIC oligomers formed in the initial stages of aggregation, although a slipped stack model for the dimer structure has been proposed that could reproduce the dimer absorption spectrum reasonably well.[20]

Another open question concerns the structure of the PIC J-aggregate. It is likely that multiple conformations exist depending on the experimental conditions, and many structural models for the aggregate have been proposed over the years.[3] For example, good fits to spectroscopic experiments have been obtained using one-dimensional aggregate models.[26–28]

In addition, electron microscopy measurements revealed tubular J-aggregates formed by the PIC dye, with a diameter of about 2.3 nm;[29,30] while this represents a major experimental advance, these techniques are not yet precise enough to image the stacking arrangement within the aggregate, and its resolution is not sufficient to observe monomers or small oligomers.

In this article, we address the above questions by means of first-principles modeling. First, using molecular dynamics simulations, we have witnessed the real-time aggregation of dye oligomers on an atomic scale, which cannot be observed experimentally; these simulations provided us with a model of the dimer structure distinct from the one proposed by Kopainsky et al.[20] Subsequently, quantum chemical calculations of transition energies and excitonic couplings, performed on the basis of the MD structures, were combined with a model for the dominant excitonic states to yield the absorption spectrum of the PIC monomer, dimer, and trimer. Comparison of this simulated dimer spectrum with experiment allowed for verification of the MD dimer structure. In particular, we have shown that the origin of the different peaks in the dimer and trimer spectra can be explained using a simple model, which fully takes into account the intricacies of the intermediate-strength vibronic coupling (exciton-phonon coupling) operative in the PIC oligomers. Our approach of using first principles calculations has the great advantage that not only can we obtain ensemble properties, but also detailed information on the time evolution of single oligomers; this turned out to be essential for understanding the structure and optical properties of the PIC dimer. Finally, several structural models for the PIC J-aggregate were tested by assessing their stability in MD simulation.

The outline of this paper is as follows. In Section II, we describe the force field and the details of the performed molecular dynamics simulations; we present our model for the excitonic states of the PIC oligomer and explain how that model is used to calculate absorption spectra. In Section III, we test our methodology by comparing simulations of the PIC crystal structure and monomer absorption spectrum to experiment. Then, we describe the outcome of our simulations of the spontaneous aggregation process and analyze the

spectral properties of the PIC dimer and trimer. We investigate the structure of the PIC J-aggregate by testing the stability of several model structures in MD simulations. In the final Section IV, we summarize and conclude.

2 Computational Details

2.1 Force Fields

2.1.1 CHARMM Drude Force Field

We performed most MD simulations using the CHARMM Drude force field,[31] which explicitly includes polarizability, unlike the modification of the GROMOS force field used in our previous work.[32,33] For water, the SWM4-NDP model was used.[34] A number of modifications had to be applied to the force field as the PIC molecule is not fully parametrized in its standard version. Therefore, the atomic charges of the PIC molecule were fitted to the molecular electrostatic potential (ESP) with the CHELPG method,[35] using version 2.9 of the Orca program. The fitting was performed using a regular grid with a spacing of 0.3 Å; grid points were included within a distance of 6 Å, but outside the COSMO van der Waals radii of the atoms. The ESP was evaluated using density functional theory with the B3LYP functional and the 6-31G* basis set, for the minimal-energy vacuum-phase geometry obtained at the same level of theory. Polarizabilities and Thole parameters (which determine the screening factor for dipole-dipole interactions between nearby atoms) for the PIC molecule's non-hydrogen atoms were taken from fully parametrized molecules containing similar chemical groups, such as pyridine and indole. Note that our procedure for obtaining atomic partial charges and atomic polarizabilities represents an approximation to the standard procedure for the CHARMM Drude force field, in which both partial charges and polarizabilities are determined in a single fitting procedure to the ESP. For bonds, angles and dihedral angles, the values of similar, already parametrized, bonds and angles were used (a full description of

the force field and associated parameter values can be found in the Supporting Information).

However, for the linker between the two quinoline moieties of the PIC molecule, no similar structures exist in the CHARMM Drude force field that could provide the parametrization. As a result, to keep the linker's carbon atom in plane with the quinoline rings to which it is bound, a harmonic potential with a force constant of $753.4\,\mathrm{kJ\,mol^{-1}\,rad^{-2}}$ was applied to dihedral angles 10-7-9-11 and 13-12-14-11 (see Figure 1 for the atom numbering). The value of this force constant was taken from our previous work on the amphi-PIC molecule,[33] which differs from the PIC molecule only in its hydrocarbon side chains. To describe correctly the twisting of the PIC molecule around its central bond, potential energy terms were added for the two dihedral angles ϕ_1 and ϕ_2, defined by atoms 10-11-13-14 and 13-11-10-9 (see Figure 1). Fitting to the quantum-chemical potential energy surface (PES, using the same methodology as in our previous work,[32] with a simplified version of the PIC molecule with ethyl tails replaced by methyl groups) yielded the energy function

$$U(\phi_1,\phi_2)/(\mathrm{kJ\,mol^{-1}}) = -8.368\cos(\phi_1) - 30\cos(2\phi_1) - 8.368\cos(\phi_2) - 30\cos(2\phi_2). \quad (1)$$

These additional potential terms lead to a great improvement in the reproduction of the quantum-chemical PES, shifting the position of the absolute minimum to approximately the correct location (PES data is supplied in the Supporting Information).

Because we observed in our preliminary MD simulations that hydrogen atoms bound to aromatic carbons of the PIC molecule were bending very much out of the plane of their respective quinoline rings, the improper force constant that keeps these hydrogens in plane was raised from 0.45 to 20 kcal $\mathrm{mol^{-1}\ rad^{-2}}$ (quantum chemical calculations for the corresponding angle in the benzene molecule resulted in an even larger force constant of 62 kcal $\mathrm{mol^{-1}\ rad^{-2}}$, but increasing the force constant to such a large value might destabilize the MD simulations).

2.1.2 GROMOS Force Field

For comparison with the CHARMM Drude force field, we have performed a small number of simulations using a modification of the GROMOS53A6 force field,[36] which is described in our previous work.[33]

2.2 Molecular Dynamics Simulations

2.2.1 MD Simulations using the CHARMM Drude Force Field

MD simulations using the CHARMM Drude force field were performed with the NAMD program.[37,38] To get rid of close contacts, all simulations were preceded by 1000 steps of conjugate gradient energy minimization, followed by a short simulation of 10 ps with a small 0.1 fs time step. Then, the time step could be increased to 0.5 fs. Attributing a small mass to the Drude particles allowed us to treat their propagation using an extended Lagrangian with a dual-Langevin thermostat; this generated a trajectory close to the self-consistent field limit.[38] The dual Langevin thermostat coupled non-Drude atoms to a heat bath at 298 K, using a damping coefficient of 20 ps^{-1}, while Drude particles were coupled to a heat bath at 1 K with a damping coefficient of 5 ps^{-1}. A Langevin barostat was used to control the pressure, with a target pressure of 1.013 25 bar, an oscillation timescale of 200 fs, and a damping timescale of 100 fs. Pressure coupling was applied isotropically in simulations of spontaneous aggregation and of separate monomers, dimers, and trimers; semi-isotropically in simulations of aggregates, with the dimension along which the aggregate was connected to its periodic image coupled separately to the pressure bath; and anisotropically to the simulation box filled half with crystal and half with water. We used periodic boundary conditions, and unless otherwise stated, a cubic simulation box with 6 nm sides.

Electrostatic forces were calculated using the Particle Mesh Ewald (PME) method, which mapped charges outside the cutoff radius of 1.2 nm to a grid, with a maximum spacing between grid points of 0.1 nm. Van der Waals forces were truncated beyond a 1.2 nm cut-

off, while a switching function was applied between 1.05 and 1.2 nm to make the van der Waals potential decrease to zero in a smooth manner. Drude particles were coupled to all non-hydrogen atoms to allow for an explicit treatment of polarization. To prevent a polarization catastrophe, an additional quartic restraining potential with a force constant of 40 000 kcal mol^{-1} Å^{-2} was applied when the bond length between a Drude particle and its parent atom exceeded 0.2 Å. To save computational effort, NAMD uses an integration scheme with multiple time steps. In our simulations, nonbonded forces were only evaluated every two time steps, based on a pair list which was updated every 10 time steps. Pairs of atoms were included in the pair list within a cutoff distance of 1.35 nm. Moreover, bonded atoms that were connected through at most one intermediate atom were excluded from non-bonded interactions (1-3 exclusion). Bond lengths within the water molecules were held fixed using the Settle algorithm.[39] In the simulations of self-aggregation and of the crystal, the screened Coulomb correction of Thole was applied to non-excluded, nonbonded pairs of Drude oscillators that were separated by less than 5 Å.

To build the starting configuration for our simulations of the PIC crystal, we used the experimentally determined crystal structure.[40] The unit cell was multiplied in the direction of the crystallographic unit vectors by factors of 5, 5, and 6, yielding a supercell (with box vectors **a**, **b**, and **c** denoted in Table 1 as 'experiment') which was used as the starting point of two MD simulations. The first simulation was performed to determine the equilibrium size of the simulation box; it had pressure coupling applied separately to all three box dimensions, and consisted of a 5 ns equilibration run followed by a 5 ns production run. A second simulation at constant volume was performed to obtain RMSD values, and consisted of a 1 ns equilibration run followed by a 3 ns production run.

To simulate the PIC monomer, we took the coordinates of a single PIC molecule and its nearest chloride counterion from the experimental crystal structure and then filled the rest of the simulation box with water. Then, we performed a 1 ns equilibration run which was the starting point for two further production trajectories: a 10 ns run with frames saved

every 250 fs, which was used for the calculation of the monomer spectrum in the static limit, and a 200 ps trajectory sampled every 2 fs, from which the spectrum was calculated with the Numerical Integration of the Schrödinger Equation (NISE) method.

For our simulations of the PIC dimer, we selected two dimers (later on referred to as dimers a and b) that showed orderly $\pi - \pi$ stacked configurations from the results of the self-aggregation simulations. Both dimers were placed in a separate simulation box, to which counterions were added at random positions before the remaining open space was filled with water. Then, 1 ns equilibration runs were performed, followed by 5 ns production runs with frames saved every 250 fs, which were later used for analysis of the dimer conformation as well as for calculating absorption spectra in the static limit. For NISE calculations of the absorption spectrum, snapshots were made of both aforementioned production runs at 0, 2.5, and 5 ns. This yielded six starting configurations for 200 ps trajectories with snapshots saved every 2 fs. For the PIC trimer, simulations were performed in the same way as for the dimer.

We constructed several aggregate geometries that were used as a starting point for MD simulations that tested the stability of these structures. One of the aggregates consisted of a single strand of 12 PIC molecules and counterions that was taken from the crystal structure and then solvated with water; the resulting size of the simulation box was 8.2 nm along the direction of the strand and 6 nm in the other two directions. Another aggregate was built of four strands from the crystal structure and contained 48 PIC molecules and counterions; at the start of the simulation, its simulation box was described by the box vectors $\mathbf{a} = (6\,\mathrm{nm}, 0, 0)$, $\mathbf{b} = (0, 6\,\mathrm{nm}, 0)$, and $\mathbf{c} = (0.11\,\mathrm{nm}, 0, 8.2\,\mathrm{nm})$. Pile-of-coins aggregates containing 20 PIC molecules were constructed by multiplying self-aggregated dimers with an orderly $\pi - \pi$ stacking into the direction perpendicular to the molecular plane, placing counterions at random locations in the box, and filling the remaining space with water. Two such aggregates were built: one with all ethyl side groups of the PIC molecules oriented in the same direction, with initial box dimensions of 8.1 nm along the direction of the aggregate

and 6 nm in the other two directions, and an aggregate with ethyl side groups on alternating sides, with box dimensions of 8.4 nm in the aggregate direction and again 6 nm in the other directions.

2.2.2 MD Simulations using the GROMOS Force Field

MD simulations utilizing our modification of the GROMOS force field were performed with the GROMACS program.[41] Newton's equations of motion were integrated using the leapfrog algorithm.[42] A time step of 1 fs was used for simulations of the PIC crystal structure, and a time step of 2 fs for simulations of self-aggregation. An atomistic description was used, except for the ethyl side groups of the PIC molecules, for which the basic building blocks were CH_2 and CH_3 groups.

The lengths of all bonds were constrained using the LINCS method, except for simulations of the crystal structure, where only bonds including hydrogen atoms were constrained.[43] Non-bonded interactions were calculated using a twin-range cutoff scheme, in which Lennard-Jones and electrostatic interactions within a cutoff distance of 0.9 nm were evaluated directly at each time step, based on a pair list recalculated every 5 steps. On the other hand, electrostatic interactions beyond the 0.9 nm cutoff radius were calculated using the PME method, with a minimal spacing between grid points of 0.12 nm, cubic interpolation and a relative strength of the Ewald-shifted direct potential at the cutoff radius of 1×10^{-5}.

Our system was coupled to a heat bath by a Berendsen thermostat[44] with a reference temperature of 298 K and a relaxation time of 0.1 ps. Pressure was controlled using a Berendsen barostat,[44] with a reference pressure of 1 bar, a relaxation time of 0.5 ps and a compressibility of 4.6×10^{-5} bar^{-1}. Pressure coupling was applied separately in all directions for the crystal simulations, while the coupling was isotropic for simulations of the spontaneous aggregation process.

The initial configurations for simulations of the self-aggregation process were prepared by randomly placing PIC molecules and counterions in the box, then adding water to fill

the remaining space. The MD simulations that tested the stability of the PIC crystal for our modification of the GROMOS force field were performed in exactly the same manner as those using the modified CHARMM Drude force field, described in the previous section, with identical trajectory lengths and sampling rates.

2.3 Exciton Hamiltonian

We used a Holstein Hamiltonian to describe the vibronic excitations of PIC monomers and oligomers. For each dye molecule, we took into account one dipole-allowed electronic excitation (the lowest-energy and optically dominant one), linearly coupled to a single harmonic vibrational mode. Thus we assume that for a monomer, the curvature of the vibrational potential remains the same upon electronic excitation, but the position of its minimum is displaced along the vibrational coordinate. Then, the Hamiltonian for one-exciton states is given by

$$H(t) = \sum_{n=1}^{N} E_n(t) b_n^\dagger b_n + \sum_{n,m=1}^{N} J_{nm}(t) b_n^\dagger b_m + \hbar\omega_0 \sum_{n=1}^{N} a_n^\dagger a_n + \hbar\omega_0 \lambda \sum_{n=1}^{N} b_n^\dagger b_n (a_n^\dagger + a_n), \qquad (2)$$

where $b_n^\dagger$ and b_n are the Pauli creation and annihilation operators of an electronic excitation at molecule n, $a_n^\dagger$ and a_n create and annihilate a vibrational energy quantum $\hbar\omega_0$ at molecule n (in the potential of the electronic ground state), E_n is the vertical excitation energy of molecule n, J_{nm} the excitonic coupling between molecules n and m, and λ^2 is the Huang-Rhys factor. Summations run over all N molecules within the oligomer. The time-dependence of the Hamiltonian is the result of fluctuations in the conformation of the molecules and the solvent environment. We assumed that these fluctuations do not affect the vibrations nor their coupling to the electronic transition.

To find the excited states of the Hamiltonian given in Eq. 2, we employed the two-particle approximation,[45] in which the full one-exciton multiphonon basis set is truncated to include only states with at most two molecules excited. In the one-particle state $|n, \tilde{\nu}\rangle$, the molecule

n is excited vibronically (i.e. electronically and vibrationally, with $\tilde{\nu}$ vibrational quanta in the displaced potential of the electronic excited state, while all the other molecules remain in their overall (electronic and vibrational) ground state. In the two-particle state $|n, \tilde{\nu}; m, \nu\rangle$, apart from the vibronically excited molecule n, one more molecule (m) is excited purely vibrationally with ν vibrational quanta in the "unshifted" potential of the electronic ground state. Thus, the excited states of the aggregate are found as linear combinations of the one- and two-particle states:

$$|k\rangle = \sum_{n} \sum_{\tilde{\nu}=0}^{\nu_{max}} c^{k}_{n,\tilde{\nu}} |n, \tilde{\nu}\rangle + \sum_{n} \sum_{m \neq n} \sum_{\tilde{\nu}=0}^{\nu_{max}-1} \sum_{\nu=1}^{\nu_{max}-\tilde{\nu}} c^{k}_{n,\tilde{\nu},m,\nu} |n, \tilde{\nu}; m, \nu\rangle. \tag{3}$$

The two-particle approach is numerically exact for dimers, as there are only two molecules constituting a dimer. It is an approximation for larger aggregates, but has been shown to perform very well for molecular aggregates and crystals.[46,47]

We further truncated the basis set size by discarding states with more than 6 phonons in total ($\tilde{\nu} + \nu$). For the monomer and dimer, we tested that increasing the cut-off for the total number of phonons beyond 6 does not change spectra in any noticable way. We used a vibrational quantum of $\hbar\omega_0$=1368 cm^{-1} and a Huang-Rhys factor of $\lambda^2 = 0.605$, following Kopainsky et al.,[20] who parametrized the vibronic states of the PIC monomer by fitting to its measured absorption spectrum.

We calculated transition energies using the semi-empirical ZINDO/S-CIS method, an accurate and computationally efficient method for calculating transition energies based on structures from MD simulations.[48] For the nuclear coordinates of the dye molecule under consideration, we used the corresponding atomic coordinates from the MD simulation snapshot. The nuclear dynamics then naturally leads to static and dynamic disorder in the transition energies. The necessary computational effort was reduced by replacing the PIC molecule's ethyl tails by hydrogen atoms, a plausible approximation since the first excited state is of π-π character. The environment was included in the form of static point charges,

with positions and charges taken from the MD trajectory. Point charges were only taken into account for molecules located within a cutoff radius of 3 nm from the center of the chromophore under consideration.

In calculating excitonic couplings, we employed the tight-binding approximation, neglecting the exchange contribution, so that the coupling J_{nm} between molecules n and m equals the Coulomb interaction between the transition charge densities of these two molecules. Couplings were calculated using the TrEsp method,[49] which approximates the transition charge density as a set of atomic transition charges fitted to best reproduce the "transition electrostatic potential".[50,51] The coupling between dye molecules m and n is then given by

$$J_{nm}(t) = \sum_{i=1}^{N_{at}} \sum_{j=1}^{N_{at}} \frac{1}{4\pi\epsilon_0} \frac{q_{mi} q_{nj}}{|\mathbf{r}_{mi}(t) - \mathbf{r}_{nj}(t)|}, \tag{4}$$

where q_{mi} and $\mathbf{r}_{mi}$ are the atomic transition charge and the position of atom i from molecule m, ϵ_0 denotes the electric permittivity of vacuum and summations run over all atoms of molecules n and m. We used the same atomic transition charges for the PIC molecule as those used previously for the *amphi*-PIC molecule,[33] since these molecules only differ in their hydrocarbon tails, which carry no transition charge. Note that transition charges were scaled to correspond with the oscillator strength of 0.678 obtained by integrating the *amphi*-PIC monomer spectrum (which is virtually identical to the PIC monomer spectrum). This oscillator strength differs from the value of 0.35 given by Kopainsky and coworkers for the PIC monomer;[20] we suspect that the difference is caused by Kopainsky et al. only taking into account the oscillator strength related to the 0-0 transition of the vibronic progression.

2.4 Absorption Spectrum in the Static Limit

The computationally most efficient way of calculating the absorption spectrum from an MD trajectory is by using the static limit, which neglects the past dynamics of each MD snapshot, thus assuming a slowly varying Hamiltonian.[52] In this limit, the absorption spectrum is given

by

$$A(\omega) \propto \sum_{ik} \langle |\boldsymbol{\mu}_{ik} \cdot \mathbf{e}|^2 \rangle f_{ik}(\omega) \tag{5}$$

where ω is the angular frequency, $\boldsymbol{\mu}_{ik}$ the transition dipole of instantaneous eigenstate k at time t_i, and $\langle \dots \rangle$ averages over the polarization directions $\mathbf{e}$ of the electromagnetic field. $f_{ik}(\omega)$ is a Lorentzian lineshape function with its mean located at the eigenenergy $\hbar\omega_{ik}$,

$$f_{ik}(\omega) = \frac{1}{\pi} \frac{\gamma}{(\hbar\omega - \hbar\omega_{ik})^2 + \gamma^2}, \tag{6}$$

where we have used a value of γ =10 cm^{-1} for the Half Width at Half Maximum (HWHM) (a value large enough to smoothen the lineshape but at the same time small enough not to influence the width of the overall spectrum). The transition dipole moments between the overall ground state and the eigenstates, $\boldsymbol{\mu}_k = \langle 0|\boldsymbol{\mu}|k\rangle$, are calculated using the expansion of $|k\rangle$ in the basis of one- and two-particle states given by Eq. 3. Since only the one-particle states have a transition dipole moment from the ground state, we obtain

$$\boldsymbol{\mu}_k = \sum_{n\tilde{\nu}} c^k_{n\tilde{\nu}} \boldsymbol{\mu}_n f_{\tilde{\nu},0}, \tag{7}$$

where the Franck-Condon factors $f_{\tilde{\nu},0}$ describe the overlap between two vibrational states, and are given by

$$f_{\tilde{\nu},0} = \frac{\lambda^{\tilde{\nu}} \exp(-\lambda^2/2)}{\sqrt{\tilde{\nu}!}}. \tag{8}$$

$\boldsymbol{\mu}_n$ denotes the transition dipole moment of molecule n, which is calculated from the atomic transition charges as

$$\boldsymbol{\mu}_n(t) = \sum_{i=1}^{N_{at}} q_{ni} \mathbf{r}_{ni}(t). \tag{9}$$

2.5 Absorption Spectrum Calculated with the NISE Method

A more accurate way to calculate the absorption spectrum is the Numerical Integration of the Schrödinger Equation (NISE) method.[53–55] This method properly accounts for the history

of each snapshot and therefore accounts for motional narrowing of spectral lines. Yet, the method is not exact, as it neglects the effect of changes in the electronic state of the dye molecules on their environment.[56] In the NISE method, the absorption spectrum is obtained from the linear response function, which is given by

$$R(t) = -\frac{i}{\hbar}\langle g(0)|\hat{\mu}(t)\hat{U}(t)\hat{\mu}(0)|g(0)\rangle\Gamma(t), \tag{10}$$

where $|g\rangle$ denotes the electronic ground state (without vibrations), $\hat{\mu}(t)$ the transition dipole operator, and the time evolution operator is given by

$$\hat{U}(t) = \exp_+\left[-\frac{i}{\hbar}\int_0^t \mathrm{d}\tau\, \hat{H}(\tau)\right], \tag{11}$$

where the exponent is positively time ordered. Decay of the electronic excitation is accounted for by the phenomenological relaxation factor $\Gamma(t) = \exp(-t/2T)$, with the lifetime of the singly excited states T =2.8 ns, as measured for the monomer of the amphi-PIC dye.[57] In order to obtain starting points for the calculation of the response function, the 200 ps MD trajectories were sampled every 20 fs. The absorption spectrum was then calculated as

$$A(\omega) = -\mathrm{Im}\int_0^\infty \mathrm{d}t\, R(t)\exp(-i\omega t). \tag{12}$$

For long times, limited sampling of the disorder in the site transition energies and the couplings causes noise in the response function. To prevent this noise from affecting the spectrum, the integral in Eq. 12 was calculated only up to 32 fs for the monomer spectrum, and up to 64 fs for the dimer and trimer spectra.

3 Results and Discussion

3.1 Testing the Force Field: Crystal Structure and Monomer Spectrum

Before we performed production MD simulations, we validated our force field by testing the stability of the experimentally determined structure of the PIC crystal, which has been obtained using X-ray structure analysis by Dammeier et al.[40] As an additional test, we simulated the absorption spectrum of the PIC monomer and compared it to the spectrum measured by Kopainsky and coworkers.[20]

To test the stability of the crystal structure in our force field, we used the experimentally determined atomic coordinates as the starting point of MD simulations. The crystal structure was then observed to remain stable in all our simulations, of which the longest lasted 15 ns. As measures for the difference between the experimentally determined crystal structure and the equilibrated structure from MD, we used the deformation of the simulation box and the root-mean-square deviation (RMSD) of the crystal coordinates from their experimental values (see Table 1). The maximal deformation of the simulation box occurred in the x-direction, perpendicular to the strands comprising the crystal, and equalled 4.5 %. The average change in unit cell dimensions was 2.2 %; for comparison, this is in the upper range of the values reported by Nemkevich et al. for a set of small molecules and for several force fields.[58] In the simulation that was used to calculate the RMSD, the size of the simulation box was fixed at the experimental value. Before analyzing the MD results, thermal fluctuations were removed by averaging atomic coordinates over all 6000 snapshots of the 3 ns trajectory. In addition, the averaged MD structure was translated and rotated separately for each group of atoms considered (PIC, chloride, or water), to minimize RMSD values. An RMSD value of 0.021 nm was obtained for the PIC molecules, several times larger than the typical values reported by Nemkevich et al.[58] This was to be expected, since the small molecules studied by Nemkevich et al. are more similar to the molecules used for parametrizing force fields

than the larger and more complex PIC molecule.

To compare the performance of the polarizable CHARMM force field with that of the nonpolarizable GROMOS force field (which we used in our previous work[32,33]) in reproducing PIC properties, we have also used the GROMOS force field to simulate the crystal structure (the results are shown in Table 1). The GROMOS force field performs considerably worse than CHARMM, resulting in significantly larger RMSD values, especially for the PIC atoms, for which the RMSD value is 2.4 times bigger than the CHARMM result. Also the deformation of the simulation box is larger for the GROMOS force field: the average change in unit cell dimensions of 3.2 % is 1.5 times bigger than the CHARMM result. We conclude that the CHARMM force field is considerably more accurate than GROMOS in reproducing the properties of the PIC crystal. This might be due to the polarizability, explicitly included in the CHARMM Drude force field but only implicitly included in GROMOS. It is well established that explicit inclusion of polarizability is important for accurate description of highly charged systems such as the PIC crystal.[59] Our finding that the nonpolarizable GROMOS force field is relatively inaccurate supports the hypothesis that the too large degree of internal disorder found in our previous work on aggregates of the amphi-PIC dye[32,33] might have been due to inaccuracy in the used force field.

While simulations of the crystal structure tested mainly the PIC-PIC interactions within our force field, the interactions between PIC chromophores and water solvent, as well as our quantum-chemical calculations of transition energies, were checked by simulating the absorption spectrum of the PIC monomer and comparing to the measured spectrum;[20] the result is shown in Figure 2. The spectrum simulated with the NISE method approximates experiment well. Relative intensities and positions of the vibronic peaks are reproduced to a good accuracy, which was to be expected since the vibronic states were parametrized by fitting to the experimental monomer spectrum. The width of the 0-0 transition is accurate except for the too large low-energy tail. We expect this tail to be caused by inaccuracies in the force field, to which quantum chemical calculations of transition energies are very sensitive.

A possible mechanism through which this inaccuracy could lead to a broadened spectrum is by causing a mismatch between MD and quantum-chemical equilibrium geometries of the chromophore.[48,60] Also, the simulated spectrum had to be blueshifted by $500\,\mathrm{cm}^{-1}$ to make its peak position coincide with experiment, due to the well-known fact that the quantum-chemical ZINDO/S method, which we used to calculate the transition energies, does not correctly reproduce absolute energy values.[48] In order to correct for this systematic error of ZINDO/S for the PIC molecule, the $500\,\mathrm{cm}^{-1}$ blueshift was applied to all simulation results shown in this work.

In the static limit, the neglect of the motional narrowing effect causes the absorption spectrum to lack the resolution needed for discerning the separate peaks of the vibronic progression, leading to a significantly poorer performance than in case of the NISE method. We also have calculated the monomer absorption spectrum in the static limit neglecting the coupling to a vibrational mode, which is practically equivalent to calculating the distribution of site transition energies (since each transition energy value contributes a Lorentzian peak with a HWHM of only $10\,\mathrm{cm}^{-1}$ to the spectrum). We can see that the transition energies fluctuate by 1000's of cm^{-1}, and that their distribution is asymmetric, with a longer tail on the low-energy side; we have previously found a similar result for the amphi-PIC dye, using a different force field than the one used here.[33] Having been convinced of our force field's accuracy by its ability to reproduce both the experimental crystal structure and the monomer absorption spectrum, we are now poised to simulate the spontaneous aggregation process.

3.2 MD Simulations of the Self-Aggregation Process

We have studied the initial phase of the self-aggregation of the PIC dye in water by means of MD simulations, starting with PIC molecules and chloride counterions randomly distributed in water. We then observed that the dye molecules spontaneously assembled into multiple oligomers, which consisted of PIC molecules stacked in a pile-of-coins fashion, as depicted

in Figure 3. The oligomers existed in a dynamic equilibrium, continuously forming, only to fall apart again later.

To quantify the amount of aggregation, we used the number of pairs of closely spaced quinolines n_q divided by the total number of molecules in the simulation box n_{mol}, as shown in Figure 4. The closely spaced quinolines were used as a measure for quinolines that are π-π stacked (these quantities are almost equal for the 0.5 nm cutoff radius we used for the quinoline center-to-center distance). To understand the meaning of this quantity, note that a face-to-face dimer has two closely spaced quinoline pairs. Thus, for a system consisting of only such dimers, $n_q/n_{mol} = 1$. For slipped dimers with only one quinoline per molecule facing its neighbor, $n_q/n_{mol} = 0.5$. Finally, if all the molecules in the box were part of a pile-of-coins aggregate with periodic boundary conditions, we would have $n_q/n_{mol} = 2$.

From Figure 4, it is clear that larger structures are formed when raising the dye concentration, in agreement with experiment.[29] The reason is that at higher concentrations, there will be more collisions due to the oligomer's Brownian motion; on the other hand, the probability of an oligomer breaking apart will not be affected by the dye concentration (as long as the dye concentration stays small enough so that oligomers do not influence each other). This causes a shift in the dynamic equilibrium, leading to larger structures. Also, our simulations show that the duration of the spontaneous aggregation process depends on the PIC concentration, with the aggregation taking place faster at higher concentrations. The aggregation lasted around 5 ns for the box with 80 PIC molecules, against 12 ns for the box of the same volume containing only 10 PIC molecules. The explanation is that at lower concentrations it takes more time before Brownian motion causes monomers or oligomers to collide, resulting in less possibilities for aggregate growth. We should note that the PIC concentrations used here are higher than in most experiments: with 10-80 PIC molecules in a 6 nm cube box, the concentration ranges from 0.077 to 0.62 M. The reason that we need a relatively high dye concentration in order to observe aggregation could be due to the limited number of dye molecules in the simulation box, which might change the dynamics

of aggregate formation. Another possibility might be that the aggregation time is in reality much longer than the simulations times we can achieve in our simulations, and we are compensating for this fact by using a higher dye concentration; this view is corroborated by a measurement of the speed of formation of the PIC J-aggregate, which was found to be of the order of a minute.[22]

The largest self-aggregated structure that formed in our simulations was a pile of coins consisting of 19 PIC molecules (shown in Figure 3a), which formed in our simulation with 80 PIC molecules; clearly, there is a considerable amount of structural disorder in its π-π stacking. With 20 PIC molecules in the simulation box, sizes ranging from monomers up to hexamers were observed, with the representative example of a tetramer depicted in Figure 3b. With 10 PICs, we observed mostly monomers and dimers. The history of the tetramer shown in Figure 3b gives a good impression of the dynamic equilibrium in which the oligomers exist: this tetramer had formed 15 ns earlier from the fusion of a trimer with a monomer. The newly formed tetramer existed as a chaotic stack for multiple nanoseconds before evolving into the more ordered stack depicted here. The monomer that took part in the tetramer formation, in turn, had broken away from a dimer 10 ns previously. The timescale of oligomer formation and breakup is thus of the order of 10 ns. Unlike in the MD simulations of *amphi*-PIC, described in our previous work,[32] most of the chloride counterions are not in close proximity to PIC oligomers, but are instead located in the bulk water.

The formation of pile-of-coins stacks as the initial step of the self-aggregation process is corroborated by spectroscopic experiments. When the PIC concentration is raised from a value where only monomers exist in those experiments, the first change to the absorption spectrum is a shift to higher energies, ascribed to the formation of dimers and possibly larger oligomers.[29,61] As we will see in Sections 3.3 and 3.4, PIC dimers and trimers which are stacked face-to-face have exactly this type of blueshifted spectrum. On the other hand, it is experimentally observed that when the dye concentration is increased further, a redshifted sharp J-band appears, polarized parallel to the aggregate axis.[29,61] Since the PIC's transition

dipole is oriented parallel to the molecule's long axis, this means that in the J-aggregate the PIC molecules must be aligned along the aggregate axis. The opposite is the case for the pile-of-coins arrangement of the oligomers observed in our simulations, where the long axis of the PIC molecule is perpendicular to the stacking direction. This means that there must be a particular aggregate size at which a structural reorganization takes place. Since we observe pile-of-coins oligomers of up to 19 molecules, our simulations of spontaneous aggregation suggest that the reorganization will take place beyond this size.

Next to our simulations utilizing the CHARMM Drude force field, we also performed simulations of the spontaneous aggregation process using a modification of the GROMOS force field. When a chloride counterion was used in these simulations, PIC oligomers formed, similar to our simulations with the CHARMM Drude force field, but with a somewhat smaller size of the PIC oligomers (less aggregation).

3.3 Absorption spectrum and geometry of the PIC Dimer

Simulation of the absorption spectrum of the PIC dimer enables us to explain the origin of the experimental dimer spectrum, while at the same time the comparison of simulated and experimental spectra tests the dimer's face-to-face stacked conformation. Our simulated dimer absorption spectrum is shown in Figure 5a, together with the spectrum that was measured by Kopainsky and coworkers.[20] In order to match the experimental positions of the peaks, we applied a redshift of $100\,\mathrm{cm}^{-1}$ (on top of the $500\,\mathrm{cm}^{-1}$ blueshift which accounts for ZINDO/S inaccuracy for PIC); this aggregation shift accounts for non-resonant interactions with higher excited states and will be taken into account for all dimer and trimer results thoughout the rest of this work. The NISE calculation reproduces the experimental spectrum to a large extent: the two peaks and the high-energy shoulder were reproduced at the correct positions and with approximately proper relative intensities. The good match between simulated and measured spectra is a strong indication of the correctness of the face-to-face conformation of the PIC dimer predicted by our MD simulations. Similar to the

situation for the monomer spectrum, the static limit is still considerably less accurate than the NISE method.

As noted above, the NISE simulation does not reproduce the relative intensities of the experimental peaks exactly. The underlying reason is revealed by plotting separately the six contributions to the NISE spectrum (each arising from a different trajectory), as done in Figure 5b. We see that there are two types of spectra, corresponding to two types of dimer conformations. One kind is formed by dimers which are orderly $\pi - \pi$ stacked, as represented by trajectories 1, 2, 4 and 6 in Figure 5b. Trajectories 3 and 5 belong to the other species, which consists of dimers in an unstable conformation; as a result of their small excitonic coupling, these dimer spectra resemble those of the monomer. Indeed, we can see in Figure 6 that the starting structures of the dimer trajectories 3 and 5 (dimer a at 5 ns and dimer b at 2.5 ns, respectively; see Section 2.1.1) are relatively weakly coupled. We conclude that the inaccuracy of relative peak intensities in the averaged spectrum is probably due to inaccuracies in the sampling of the $\pi - \pi$ stacked and weakly coupled dimer species: comparing Figures 5a and 5b, we can see that the contribution of the weakly coupled species is underrepresented. Surprisingly, this suggests that the amount of time the dimer spends in a disordered and unstable conformation is even more than the two out of six instances that we sampled.

To get better insight into the origin of the peaks in the absorption spectrum of the ordered, strongly coupled PIC dimer we performed a detailed analysis of the excited states of a model dimer. This revealed that the experimental dimer spectrum, which consists of two peaks followed by a high energy shoulder, can be interpreted as originating mostly from excitations with an in-phase combination of transition dipole moments, accompanied by 0, 1, and 2 phonons, respectively. As is typical for H-aggregates, these states are blueshifted with respect to the monomer. The parameters for the model dimer were obtained by averaging over the representative trajectory 6, which yielded an excitonic coupling of $J = 956$ cm^{-1} and a 15° angle between the transition dipole moments of the two PIC molecules. The

excitation energies of both molecules were assumed equal and taken as $18\,904\,\mathrm{cm}^{-1}$, which is the average value over both molecules from trajectory 6 (including both the blueshift due to ZINDO/S inaccuracies and the dimerization redshift); this assumption significantly simplifies the interpretation, as the excited states of a dimer can now be classified as either symmetric (+) or antisymmetric (-) with respect to exchange of the two PIC molecules:

$$|k_{\pm}\rangle = \sum_{\tilde{\nu}=0}^{\nu_{max}} c^{k}_{\pm,\tilde{\nu}} \left(|1,\tilde{\nu}\rangle \pm |2,\tilde{\nu}\rangle\right) + \sum_{\tilde{\nu}=0}^{\nu_{max}-1} \sum_{\nu=1}^{\nu_{max}-\tilde{\nu}} c^{k}_{\pm,\tilde{\nu},\nu} \left(|1,\tilde{\nu};2,\nu\rangle \pm |2,\tilde{\nu};1,\nu\rangle\right). \qquad (13)$$

The stick spectrum of this model dimer is shown in Figure 5b. Because of the small angle between the transition dipole moments of the two PIC molecules, the majority of the absorption intensity is carried by the transitions to symmetric states. The apparent discrepancy between the positions of the sticks and the maxima of the NISE-simulated spectrum for trajectory 6 is a result of our assumption of equal excitation energies of the two molecules building the dimer. When disorder is included, the symmetric and antisymmetric states of the dimer are coupled; in effect the eigenstates are pushed away from each other: the low intensity antisymmetric states shift to lower energies while the intense symmetric ones shift to higher energies, thus shifting the overall spectrum to higher energies.

As is typical for an H-type dimer, the lowest-energy excitation, at about $18\,200\,\mathrm{cm}^{-1}$ is to the antisymmetric state, with a total of 0 vibrational quanta (with a small, 6 % admixture, of the state with 1 vibrational quantum); however, due to its small transition dipole moment this excitation contributes only little to the low-energy tail of the absorption spectrum. Most of the intensity of the first peak arises from the transition to the symmetric state, located at an energy of about $19\,200\,\mathrm{cm}^{-1}$. While being mostly (74 %) 0-phonon state, it contains a significant admixture (20 %) of the 1-phonon states of both one- and two-particle origin, that is states where the vibration is excited on the same molecule as the electronic excitation, as well as states with a vibration on the electronically unexcited molecule. The second absorption peak originates mostly from the excitation to the symmetric state with

1 vibrational quantum (76 %) at about 20 600 cm^{-1}, with a substantial admixture of the 0-phonon state (22 %). This state has considerable contribution from 2-particle states (39 %). The high-energy shoulder arises from the transition to a symmetric state with a transition energy of about 22 000 cm^{-1} and with 2 vibrational quanta (76 %), mixed with a state with 1 vibrational quantum (23 %). The contribution from states with vibrations excited on the molecule which is in its electronic ground state (2-particle states) is even higher and reaches 51 %. The interpretation given above remains valid for the other 3 trajectories which correspond to strongly coupled dimers (trajectories 1, 2, and 4); the excitation energies differ from those of trajectory 6 by at most 170 cm^{-1}, while the contributions from states with different numbers of phonons change by no more than 6 %.

The non-negligible mixing of states with a different number of vibrational quanta, as well as the significant 2-particle character of the intensity-carrying states, are a signature of the breakdown of the strong vibronic coupling limit. This is not surprising, since the combination of having an average coupling $J = 956$ cm^{-1}, a vibrational quantum $\hbar\omega_0 = 1368$ cm^{-1}, and a Huang-Rhys factor of 0.605 makes the PIC dimer an excellent example of intermediate vibronic coupling. The effects are manifested as the strongly altered absorption intensity distribution as compared to the monomer, and as the increased splitting between the 0-0 and 0-1 line.[62–64]

The time evolution of the dimer conformation can be studied by tracking the excitonic coupling, the angle between the two monomeric transition dipoles, and the PIC molecules' separation (taken as the distance between the two molecules' linker carbon atoms). The time dependence of these quantities is shown in Figure 6, for the two production runs that were also used to calculate the dimer absorption spectrum in the static limit. All three quantities are highly correlated, as we will discuss in more detail using dimer b as an example. Initially, the two PIC molecules are π-π stacked in an ordered manner (as depicted in Figure 7a); the coupling is strong and negative, which is due to the antiparallel orientation of the transition

dipoles. * As should be the case for a dimer in a stable π-π stacked conformation, the center-to-center separation is small, only about 0.5 nm. At around 200 ps, one of the PIC molecules starts rotating around its long axis (see Figure 7b). At the time of rotation, a temporary increase in the center-to-center distance to 0.7 nm and a decreasing alignment of the transition dipoles is accompanied by a drop in the coupling strength. The dimer quickly returns to a stable state (Figure 7c), the excitonic coupling is strong, but now the ethyl sidegroups of the two dyes point in opposite directions. After 1 ns of simulation time, the dimer enters an unstable, weakly coupled state (shown in Figure 7d), which lasts about 2 ns. During this time, the alignment of the transition dipoles deteriorates, the separation between the chromophores increases up to 0.9 nm, and as a result, the coupling strength oscillates around zero. Between 3 ns and 5 ns, the dimer is again in a stable state; during the unstable period, one of the transition dipoles has turned around, resulting in a parallel orientation which makes the coupling positive.

The PIC dimer is thus a highly volatile arrangement, which periodically leaves its stable π-π stacked structure and enters an unstable state, to return to stability soon after. The relative orientation of the transition dipoles, as well as that of the ethyl sidegroups, changes on a nanosecond timescale. This means that it is not accurate to model the dimer structure using a single value for the angle between the transition dipoles, as was done previously by Kopainsky and coworkers in their seminal work on the PIC dimer.[20] The importance of taking into account the variation in dimer conformations is demonstrated by the fact that Kopainsky et al. probably proposed an incorrect model structure based on their single, effective value of 70° for the angle between the transition dipoles: they suggested a sandwich dimer with only a single quinoline of each molecule π-π stacked to the other dye, instead of the structure with the whole dye molecule stacked face to face as found in this work. Note that even though we conclude on a different dimer model than Kopainsky et al., the average

*Even though the coupling is negative, this still is an H-dimer, as the optically allowed state is now (approximately) antisymmetric with respect to interchange of both molecules and therefore occurs above the monomer transition.

absolute value of the coupling in our simulations, 641 cm^{-1} for dimer a and 584 cm^{-1} for dimer b, is very similar to their effective value of 630 cm^{-1}.[20]

3.4 Absorption spectrum of the PIC Trimer

We further investigated the self-aggregation process by simulating the absorption spectrum of the PIC trimer, shown in Figure 8a. As we did for the dimer, we applied an aggregation redshift of 100 cm^{-1} to all calculated trimer spectra (as well as a 500 cm^{-1} blueshift to correct for ZINDO/S systematic error). The trimer spectrum is qualitatively similar to that of the dimer, consisting of two peaks and a high-energy shoulder. The second, most intense peak of the NISE-simulated trimer spectrum lies 370 cm^{-1} higher than the corresponding peak of the dimer. This additional blueshift results from the coupling to a third chromophore; it is considerably smaller than the shift of 1620 cm^{-1} between the main peaks of the experimental monomer and dimer spectra. To investigate the variability of the NISE spectra between different trimer trajectories, we have plotted them for all six trimer trajectories that were averaged over to obtain the trimer absorption discussed above, as shown in Figure 8b. We see that the intensity of the first peak (around 19 200 cm^{-1}) is relatively large for some trajectories, and that these trajectories also show a somewhat smaller blueshift of their most intense peak; during these trajectories the $\pi - \pi$ stacking must have been relatively weak. Note that there are no trajectories that have a spectrum similar to that of the monomer, in contrast to the dimer result depicted in Figure 5b; this must be caused by the trimer having two nearest-neighbor pairs instead of one, so that the chance is small that both pairs are simultaneously weakly coupled.

Similarly as for the dimer, we performed a detailed analysis of the eigenstates of a model trimer, for which the parameters were obtained by averaging over trajectory 4 (which yields the spectrum closest to the overall average). This resulted in an excitation energy (corrected for the ZINDO/S blueshift and aggregation redshift) of 19 105 cm^{-1}, excitonic couplings between the nearest neighbors of -832 cm^{-1}, and between the second neighbors of 205 cm^{-1}.

The angle between the transition dipoles was taken as 157° and 45° for the nearest and second neighbors, respectively. Tentatively, the interpretation of the three peaks visible in the absorption spectrum is similar as in the dimer case, with the lowest peak resulting from 0-0 vibronic transitions associated with the three exciton states of the trimer, the second peak being predominantly the first vibronic replica, and the third peak being mostly the second vibronic replica. However, as the exciton bandwidth increases for the trimer as compared to the dimer, we move further away from the strong vibronic coupling regime towards the strong electronic coupling regime. In effect, for the trimer, both the description in the displaced oscillator basis of the strong vibronic coupling, as well as in the undisplaced oscillator basis of the weak vibronic coupling is cumbersome, and strong mixing of states characterized by different numbers of phonons is observed. We will present here the general picture, without going into intricacies of the intermediate coupling.

The lowest peak in the trimer absorption spectrum results from the transition between the ground state and three different excited states with 0 vibrational quanta. The lowest-energy one, at approximately $18\,100\,\mathrm{cm}^{-1}$, is associated with the exciton characterized by approximately out-of-phase transition dipoles. This out-of-phase character results from a combination of in-phase wavefunction amplitudes and an almost antiparallel orientation of the nearest neighbor transition dipoles (see above). As typical for H-aggregates it carries little oscillator strength and thus forms a low-energy tail of the first absorption peak. A larger contribution comes from the second excitation at around $18\,700\,\mathrm{cm}^{-1}$, to a state related to the exciton characterized by a node on the central molecule. Most of the intensity of the first peak is carried by a transition at about $19\,000\,\mathrm{cm}^{-1}$ to the exciton state for which the transition dipoles are all in phase (which is a result of out-of-phase wavefunction amplitudes combined with almost antiparallel transition dipoles on nearest neighbors). With the growing energy of those states the admixture of one-phonon states grows (from about 7% to 26%), as does the two-particle character of the excitations (from 4% to 17%).

Most of the intensity of the second peak comes from the excitation at $20\,800\,\mathrm{cm}^{-1}$ of

the state which is mostly (70%) an in-phase combination of the electronic excited states of all molecules accompanied by a single vibrational excitation, with a considerable admixture (18%) of 0-phonon states. Compared to the situation in the dimer, the two-particle contribution is larger (54%). The third peak (a shoulder on the high-energy side of the main peak) is due to the 2-phonon states, considerably mixed with 1- and 3-phonon states.

Comparing the calculated trimer spectrum to experimental data might give us information on its abundance in experiment. To this end, in Figure 8a we have plotted the simulated trimer spectrum together with the experimental dimer spectrum and the spectrum measured at the onset of J-aggregation. It is clear that at the onset of aggregation, large contributions to the spectrum are made by the PIC dimer and J-aggregate. However, the accuracy of available data is not sufficient to determine if there are also smaller contributions from trimers, larger oligomers, or monomers. If these species exist at the onset of aggregation, it seems likely that they will be far less prevalent than the dimer.

From Figure 8a we can see that the static limit result for the trimer absorption spectrum approaches the more accurate NISE result; in contrast, the static limit performed significantly worse than NISE for the monomer and dimer (see Figures 2 and 5a). The static limit thus seems to become increasingly accurate with increasing oligomer size. Two mechanism may be at play. First, exchange narrowing starts playing a role with increasing oligomer size, and this might diminish the importance of the motional narrowing which is neglected in the static limit. Second, the separation between the most intense peaks increases from $1290\,\mathrm{cm}^{-1}$ for the monomer, to $1494\,\mathrm{cm}^{-1}$ for the dimer, and to $1857\,\mathrm{cm}^{-1}$ for the trimer (the values are given here for the NISE results). This increased separation will make each distinct peak more visible, even when the static limit overestimates the width of individual peaks.

3.5 Stability of PIC Aggregates

Our simulations of the spontaneous aggregation process did not show a structural transition from H-oligomers with a pile-of-coins geometry to large J-aggregates. Therefore, we took

a different route to investigate the structure of the PIC aggregate: we tested the stability of model structures in MD simulation. We chose four promising structural motifs for the PIC aggregate: (1) a pile-of-coins geometry with all ethyl side groups of the PIC molecules located on the same side of the aggregate, (2) a pile-of-coins geometry with ethyl side groups of neighboring dyes located on alternate sides of the aggregate, depicted in Figure 9a, (3) a single strand from the experimentally determined crystal structure, which was used in the past as a one-dimensional model of the J-aggregate,[65] shown in Figure 9b, (4) a thread consisting of four such strands, suggested by cryo-TEM images of rodlike PIC aggregates from von Berlepsch et al.,[29] depicted in Figure 9c. Structures (1) and (2) were suggested by our simulations of the self-aggregation process, and are similar to the previously proposed 'staircase' model of a slipped stack of dyes.[66] All aggregates were connected to their periodic images in the direction of the aggregate axis, which should greatly diminish any finite size effects. Unfortunately, none of the investigated aggregate types turned out to be stable. The strands from the crystal structure fell apart into a number of oligomers with a pile-of-coins geometry, which were similar to those formed in our simulations of the spontaneous aggregation process, and the pile-of-coins aggregate broke apart into smaller segments. To make sure that any assembly of strands from the crystal is unstable in our force field, an MD simulation was performed with half the box occupied by the crystal structure and half filled with water solvent. The result was that the crystal started falling apart; within 20 ns, most of the crystal had dissolved into the water to form pile-of-coins oligomers, as shown in Figure 10.

Our simulations thus suggest that PIC aggregates do not consist of strands like those in the crystal structure, where the quinoline rings are π-π stacked in a parallel-displaced manner, nor do they have a pile-of-coins geometry. An alternative could be that the rods imaged by Berlepsch et al. are cylinders consisting of a monolayer or a bilayer of PIC molecules (where in the bilayer the ethyl tails would be shielded from the water solvent); this type of structure has been used successfully to explain the spectroscopy of the C8S3

aggregate.[67] On the other hand, we cannot exclude the possibility of a realistic aggregate structure being unstable in our MD simulations, due to the approximate nature of the force field approach.

4 Conclusions

We have studied the initial steps of the spontaneous aggregation process of the PIC dye in water using MD simulations and spectral modeling. First, we tested our methodology by verifying the stability of the experimental structure of the PIC crystal in our force field, and by comparing the simulated absorption spectrum of the PIC monomer to experiment. We learned that the CHARMM Drude force field used in this work reproduces the PIC crystal structure considerably better than the GROMOS force field used in our previous work on the related amphi-PIC dyes.[32,33] Then, we performed molecular dynamics simulations of the self-aggregation process, in which pile-of-coins stacks of up to 19 dyes were formed.

The dimer spectrum compared favorably to experiment, corroborating the simulated dimer's face-to-face stacked geometry, which differs from the classical structure proposed by Kopainsky et al.[20] The dimer structure was found to be very flexible, switching between a stable $\pi - \pi$ stacked state and a weakly coupled state every few nanoseconds. This fact has important implications for the dimer absorption spectrum, which turns out to be a superposition of two types of lineshapes: one belonging to an orderly $\pi-\pi$ stacked structure, and one similar to the monomer lineshape of the weakly coupled dimer. Taking into account structural fluctuations thus turns out to be essential for understanding the dimer spectrum. In contrast, the spectral contribution of orderly $\pi-\pi$ stacked structures could be understood using a static vibronic model, which allowed us to elucidate the origin of each peak observed in experiment, and showed that the dimer resides in the intermediate vibronic coupling regime. Next, we simulated the trimer spectrum and compared it to the experimental spectrum at the onset of J-aggregation, from which we could conclude that in experiment trimers and

larger oligomers, if they are present at all, are probably not prevalent.

It is difficult to assess up to which size pile-of-coins oligomers grow in experiment. The experimental spectrum that we used does not give any evidence for the existence of H-type structures larger than the dimer at the onset of aggregation; on the other hand, it is difficult to believe that there are no intermediate structures between H-type dimers and large J-aggregates. Additional insights might be gained using novel spectroscopic techniques such as 2D spectroscopy, which can help determine which spectral peaks are due to the aggregate and which to other species at the onset of aggregation. In addition to the process by which aggregates are formed, also the aggregate structure remains an open question.

Acknowledgement

F.H. thanks Alex H. de Vries for several insightful discussions.

Supporting Information Available

In the Supporting Information, we provide data on the potential energy surface for the PIC linker, calculated with the quantum-chemical DFT method, and the CHARMM Drude force field with and without inclusion of additional potential terms for the linker. In addition, we provide files containing the used CHARMM Drude force field parameters and an NAMD input file containing parameters of a representative MD simulation. This material is available free of charge via the Internet at `http://pubs.acs.org/`.

References

(1) Scheibe, G. *Angew. Chem.* **1936**, *49*, 563–563.

(2) Jelley, E. E. *Nature* **1936**, *138*, 1009–1010.

(3) Würthner, F.; Kaiser, T. E.; Saha-Möller, C. R. J-Aggregates: From Serendipitous

Discovery to Supramolecular Engineering of Functional Dye Materials. *Angew. Chem. Int. Ed.* **2011**, *50*, 3376–3410.

(4) Kobayashi, T., Ed. *J-Aggregates*; World Scientific, 2012; Vol. 2.

(5) Mees, C. E. K. *The Theory of the Photographic Process*; The MacMillan Company: New York, 1962.

(6) Tani, T. *Photographic Sensitivity*; Oxford University Press: Oxford, U.K., 1995.

(7) Kirstein, S.; Daehne, S. J-Aggregates of Amphiphilic Cyanine Dyes: Self-Organization of Artificial Light Harvesting Complexes. *Int. J. Photoenergy* **2006**, *2006*, 1–21.

(8) Knoester, J.; Daehne, S. Prospects of Artificial Light Harvesting Systems: An Introduction. *Int. J. Photoenergy* **2006**, *2006*, 1–3.

(9) Lidzey, D. G.; Bradley, D. D. C.; Skolnick, M. S.; Virgili, T.; Walker, S.; Whittaker, D. M. Strong Exciton-Photon Coupling in an Organic Semiconductor Microcavity. *Nature* **1998**, *395*, 53–55.

(10) Bradley, M. S.; Bulović, V. Intracavity Optical Pumping of J-Aggregate Microcavity Exciton Polaritons. *Phys. Rev. B* **2010**, *82*, 033305.

(11) Bogdanov, V. L.; Viktorova, E. N.; Kulya, S. V.; Spiro, A. S. Nonlinear Cubic Susceptibility and Dephasing of Exciton Transitions in Molecular Aggregates. *JETP Lett.* **1991**, *53*, 105–108.

(12) Wang, Y. Resonant Third-Order Optical Nonlinearity of Molecular Aggregates with Low-Dimensional Excitons. *J. Opt. Soc. Am. B* **1991**, *8*, 981–985.

(13) Spano, F. C.; Mukamel, S. Cooperative Nonlinear Optical Response of Molecular Aggregates: Crossover to Bulk Behavior. *Phys. Rev. Lett.* **1991**, *66*, 1197–1200.

(14) Knoester, J. Third-Order Optical Response of Molecular Aggregates. Disorder and the Breakdown of Size-Enhancement. *Chem. Phys. Lett.* **1993**, *203*, 371–377.

(15) Klugkist, J. A.; Malyshev, V. A.; Knoester, J. Intrinsic Optical Bistability of Thin Films of Linear Molecular Aggregates: The One-Exciton Approximation. *J. Chem. Phys.* **2007**, *127*, 164705.

(16) Mukhopadhyay, S.; Risko, C.; Marder, S. R.; Brédas, J.-L. Polymethine Dyes for All-Optical Switching Applications: a Quantum-Chemical Characterization of Counter-Ion and Aggregation Effects on the Third-Order Nonlinear Optical Response. *Chem. Sci.* **2012**, *3*, 3103–3112.

(17) van Amerongen, H.; Valkunas, L.; van Grondelle, R. *Photosynthetic Excitons*; World Scientific: Singapore, 2000.

(18) Ritz, T.; Damjanović, A.; Schulten, K. The Quantum Physics of Photosynthesis. *ChemPhysChem* **2002**, *3*, 243–248.

(19) Ganapathy, S.; Oostergetel, G. T.; Wawrzyniak, P. K.; Reus, M.; Gomez Maqueo Chew, A.; Buda, F.; Boekema, E. J.; Bryant, D. A.; Holzwarth, A. R.; de Groot, H. J. M. Alternating Syn-Anti Bacteriochlorophylls form Concentric Helical Nanotubes in Chlorosomes. *Proc. Natl. Acad. Sci. U.S.A.* **2009**, *106*, 8525–8530.

(20) Kopainsky, B.; Hallermeier, J. K.; Kaiser, W. The First Step of Aggregation of PIC. The Dimerization. *Chem. Phys. Lett.* **1981**, *83*, 498–502.

(21) Kopainsky, B.; Hallermeier, J.; Kaiser, W. On the Aggregates of Pseudoisocyanine Chloride (PIC). *Chem. Phys. Lett.* **1982**, *87*, 7 – 10.

(22) Pasternack, R. F.; Fleming, C.; Herring, S.; Collings, P. J.; dePaula, J.; DeCastro, G.; Gibbs, E. J. Aggregation Kinetics of Extended Porphyrin and Cyanine Dye Assemblies. *Biophys. J.* **2000**, *79*, 550 – 560.

(23) Kitahama, Y.; Yago, T.; Furube, A.; Katoh, R. Formation Process of Micrometer-Sized Pseudoisocyanine J-aggregates Studied by Single-Aggregate Fluorescence Spectroscopy. *Chem. Phys. Lett.* **2008**, *457*, 427 – 433.

(24) West, W.; Pearce, S. The Dimeric State of Cyanine Dyes. *J. Phys. Chem.* **1965**, *69*, 1894–1903.

(25) Nemeth, A.; Lukes, V.; Sperling, J.; Milota, F.; Kauffmann, H. F.; Mancal, T. Two-dimensional Electronic Spectra of an Aggregating Dye: Simultaneous Measurement of Monomeric and Dimeric Line-shapes. *Phys. Chem. Chem. Phys.* **2009**, *11*, 5986–5997.

(26) Fidder, H.; Knoester, J.; Wiersma, D. A. Observation of the One-Exciton to Two-Exciton Transition in a J-Aggregate. *J. Chem. Phys.* **1993**, *98*, 6564–6566.

(27) Heijs, D. J.; Malyshev, V. A.; Knoester, J. Decoherence of Excitons in Multichromophore Systems: Thermal Line Broadening and Destruction of Superradiant Emission. *Phys. Rev. Lett.* **2005**, *95*, 177402–177405.

(28) Augulis, R.; Malyshev, A. V.; Malyshev, V. A.; Pugžlys, A.; Knoester, J.; van Loosdrecht, P. H. M. Quest for Order in Chaos: Hidden Repulsive Level Statistics in Disordered Quantum Nanoaggregates. *J. Phys. Chem. Lett.* **2010**, *1*, 2911–2916.

(29) von Berlepsch, H.; Böttcher, C.; Dähne, L. Structure of J-Aggregates of Pseudoisocyanine Dye in Aqueous Solution. *J. Phys. Chem. B* **2000**, *104*, 8792–8799.

(30) von Berlepsch, H.; Böttcher, C. Network Superstructure of Pseudoisocyanine J-Aggregates in Aqueous Sodium Chloride Solution Revealed by Cryo-Transmission Electron Microscopy. *J. Phys. Chem. B* **2002**, *106*, 3146–3150.

(31) Lamoureux, G.; Roux, B. Modeling Induced Polarization with Classical Drude Oscillators: Theory and Molecular Dynamics Simulation Algorithm. *J. Chem. Phys.* **2003**, *119*, 3025–3039.

(32) Haverkort, F.; Stradomska, A.; de Vries, A. H.; Knoester, J. Investigating the Structure of Aggregates of an Amphiphilic Cyanine Dye with Molecular Dynamics Simulations. *J. Phys. Chem. B* **2013**, *117*, 5857–5867.

(33) Haverkort, F.; Stradomska, A.; de Vries, A. H.; Knoester, J. First Principles Calculation of the Optical Properties of an Amphiphilic Cyanine Dye Aggregate. *J. Phys. Chem. A* **2014**, *118*, 1012.

(34) Lamoureux, G.; Harder, E.; Vorobyov, I. V.; Roux, B.; MacKerell Jr., A. D. A Polarizable Model of Water for Molecular Dynamics Simulations of Biomolecules. *Chem. Phys. Lett.* **2006**, *418*, 245 – 249.

(35) Breneman, C. M.; Wiberg, K. B. Determining Atom-Centered Monopoles from Molecular Electrostatic Potentials. The Need for High Sampling Density in Formamide Conformational Analysis. *J. Comput. Chem.* **1990**, *11*, 361–373.

(36) Oostenbrink, C.; Villa, A.; Mark, A. E.; van Gunsteren, W. F. A Biomolecular Force Field Based on the Free Enthalpy of Hydration and Solvation: The GROMOS Force-Field Parameter Sets 53A5 and 53A6. *J. Comput. Chem.* **2004**, *25*, 1656–1676.

(37) Phillips, J. C.; Braun, R.; Wang, W.; Gumbart, J.; Tajkhorshid, E.; Villa, E.; Chipot, C.; Skeel, R. D.; Kalé, L.; Schulten, K. Scalable Molecular Dynamics with NAMD. *J. Comput. Chem.* **2005**, *26*, 1781–1802.

(38) Jiang, W.; Hardy, D. J.; Phillips, J. C.; MacKerell, A. D.; Schulten, K.; Roux, B. High-Performance Scalable Molecular Dynamics Simulations of a Polarizable Force Field Based on Classical Drude Oscillators in NAMD. *J. Phys. Chem. Lett.* **2011**, *2*, 87–92.

(39) Miyamoto, S.; Kollman, P. A. Settle: An Analytical Version of the SHAKE and RATTLE Algorithm for Rigid Water Models. *J. Comput. Chem.* **1992**, *13*, 952–962.

(40) Dammeier, B.; Hoppe, W. Die Kristall- und Molekülstruktur von *N,N'*-Diäthylpseudoisocyaninchlorid. *Acta Crystallogr. Sect. B* **1971**, *27*, 2364–2370.

(41) Hess, B.; Kutzner, C.; van der Spoel, D.; Lindahl, E. GROMACS 4: Algorithms for Highly Efficient, Load-Balanced, and Scalable Molecular Simulation. *J. Chem. Theory Comput.* **2008**, *4*, 435–447.

(42) Hockney, R. W. The Potential Calculation and some Applications. *Meth. Comput. Phys.* **1970**, *9*, 136–211.

(43) Hess, B.; Bekker, H.; Berendsen, H. J. C.; Fraaije, J. G. E. M. LINCS: a Linear Constraint Solver for Molecular Simulations. *J. Comput. Chem.* **1997**, *18*, 1463–1472.

(44) Berendsen, H. J. C.; Postma, J. P. M.; van Gunsteren, W. F.; DiNola, A.; Haak, J. R. Molecular Dynamics with Coupling to an External Bath. *J. Chem. Phys.* **1984**, *81*, 3684–3690.

(45) Philpott, M. R. Theory of the Coupling of Electronic and Vibrational Excitations in Molecular Crystals and Helical Polymers. *J. Chem. Phys.* **1971**, *55*, 2039–2054.

(46) Spano, F. C. Absorption and Emission in Oligo-Phenylene Vinylene Nanoaggregates: The Role of Disorder and Structural Defects. *J. Chem. Phys.* **2002**, *116*, 5877–5891.

(47) Stradomska, A.; Petelenz, P. Intermediate Vibronic Coupling in Sexithiophene Single Crystals. II. Three-Particle Contributions. *J. Chem. Phys.* **2009**, *131*, 044507.

(48) Zwier, M. C.; Shorb, J. M.; Krueger, B. P. Hybrid Molecular Dynamics-Quantum Mechanics Simulations of Solute Spectral Properties in the Condensed Phase: Evaluation of Simulation Parameters. *J. Comput. Chem.* **2007**, *28*, 1572–1581.

(49) Madjet, M. E.; Abdurahman, A.; Renger, T. Intermolecular Coulomb Couplings from Ab Initio Electrostatic Potentials: Application to Optical Transitions of Strongly Cou-

pled Pigments in Photosynthetic Antennae and Reaction Centers. *J. Phys. Chem. B* **2006**, *110*, 17268–17281.

(50) Sigfridsson, E.; Ryde, U. Comparison of Methods for Deriving Atomic Charges from the Electrostatic Potential and Moments. *J. Comput. Chem.* **1998**, *19*, 377–395.

(51) Sigfridsson, E.; Ryde, U.; Bush, B. L. Restrained Point-Charge Models for Disaccharides. *J. Comput. Chem.* **2002**, *23*, 351–364.

(52) Mukamel, S. *Principles of Nonlinear Optical Spectroscopy*; Oxford University Press: New York, 1995.

(53) Jansen, T. l. C.; Knoester, J. Nonadiabatic Effects in the Two-Dimensional Infrared Spectra of Peptides: Application to Alanine Dipeptide. *J. Phys. Chem. B* **2006**, *110*, 22910–22916.

(54) Jansen, T. l. C.; Knoester, J. Waiting Time Dynamics in Two-Dimensional Infrared Spectroscopy. *Accounts of Chemical Research* **2009**, *42*, 1405–1411.

(55) Roden, J.; Eisfeld, A.; Wolff, W.; Strunz, W. T. Influence of Complex Exciton-Phonon Coupling on Optical Absorption and Energy Transfer of Quantum Aggregates. *Phys. Rev. Lett.* **2009**, *103*, 058301.

(56) Tempelaar, R.; van der Vegte, C. P.; Knoester, J.; Jansen, T. l. C. Surface Hopping Modeling of Two-Dimensional Spectra. *J. Chem. Phys.* **2013**, *138*.

(57) Lang, E.; Sorokin, A.; Drechsler, M.; Malyukin, Y. V.; Köhler, J. Optical Spectroscopy on Individual amphi-PIC J-Aggregates. *Nano Lett.* **2005**, *5*, 2635–2640.

(58) Nemkevich, A.; Bürgi, H.-B.; Spackman, M. A.; Corry, B. Molecular Dynamics Simulations of Structure and Dynamics of Organic Molecular Crystals. *Phys. Chem. Chem. Phys.* **2010**, *12*, 14916–14929.

(59) Lopes, P. E. M.; Roux, B.; MacKerell Jr, A. D. Molecular Modeling and Dynamics Studies with Explicit Inclusion of Electronic Polarizability: Theory and Applications. *Theor. Chem. Acc.* **2009**, *124*, 11–28.

(60) Jing, Y.; Zheng, R.; Li, H.-X.; Shi, Q. Theoretical Study of the Electronic-Vibrational Coupling in the Q_y States of the Photosynthetic Reaction Center in Purple Bacteria. *J. Phys. Chem. B* **2012**, *116*, 1164–1171.

(61) Scheibe, G.; Kandler, L. Anisotropie Organischer Farbstoffmoleküle. Nebenvalenz-Bindung als Energieüberträger. *Naturwissenschaften* **1938**, *24/25*, 412–413.

(62) Witkowski, A.; Moffitt, W. Electronic Spectra of Dimers: Derivation of the Fundamental Vibronic Equation. *J. Chem. Phys. 33*, 872.

(63) Fulton, R. L.; Gouterman, M. Vibronic Coupling. II. Spectra of Dimers. *J. Chem. Phys.* **1964**, *41*, 2280.

(64) Andrzejak, M.; Petelenz, P. Vibronic Coupling in Dimer - A Convenient Approximation Revisited. *Chem. Phys.* **2007**, *335*, 155 – 163.

(65) Daltrozzo, E.; Scheibe, G.; Geschwind, K.; Haimerl, F. *Photogr. Sci. Eng.* **1974**, *18*, 441–450.

(66) Scheibe, G.; Haimerl, F.; Hoppe, W. Über die Ursache des Cirkulardichroismus der Reversibel Polymeren des Pseudoisocyanins. *Tetrahedron Lett.* **1970**, *11*, 3067.

(67) Eisele, D. M.; Cone, C. W.; Bloemsma, E. A.; Vlaming, S. M.; van der Kwaak, C. G. F.; Silbey, R. J.; Bawendi, M. G.; Knoester, J.; Rabe, J. P.; Vanden Bout, D. A. Utilizing Redox-Chemistry to Elucidate the Nature of Exciton Transitions in Supramolecular Dye Nanotubes. *Nature Chem.* **2012**, *4*, 655–662.

Table 1: Assessment of the accuracy of the CHARMM Drude force field used in this work, and of a modified version of the GROMOS force field used in our previous work,[33] by testing the stability of the experimentally determined crystal structure in these force fields. The upper part of the table shows the root-mean-square deviation (RMSD) between simulated and experimental crystal structures. The lower part conveys the simulated and measured sizes of the simulation box, with the relative deviation of simulated values from experiment given in parentheses. Only nonzero components of the box vectors a, b, and c are given.

RMSD / nm	PIC	chloride	water	
CHARMM Drude	0.021	0.019	0.019	
GROMOS	0.051	0.026	0.036	
box size / nm (error)	a_x	b_x	b_y	c_z
experiment	6.793	0.09375	6.853	6.310
CHARMM Drude	7.1 (4.5 %)	0.097 (3.5 %)	6.9 (0.69 %)	6.4 (1.4 %)
GROMOS	7.0 (3.0 %)	0.097 (3.5 %)	7.1 (3.6 %)	6.5 (3.0 %)

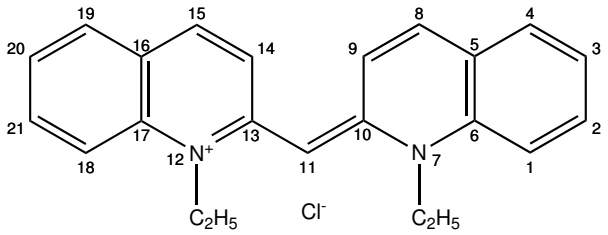

Figure 1: The PIC dye with chloride counterion.

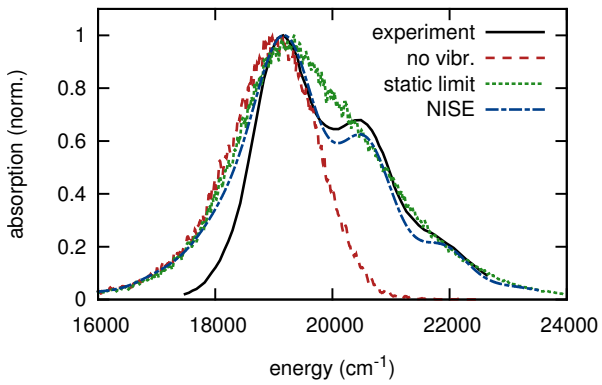

Figure 2: Absorption spectrum of the PIC monomer, according to experiment[20] (black solid curve) as well as our simulations at various levels of sophistication: NISE with explicit coupling to vibrations (blue long/short dashes), static limit with vibrations (green short dashes), and static limit without vibrations (red dashed curve). Absorption maxima were normalized to unity.

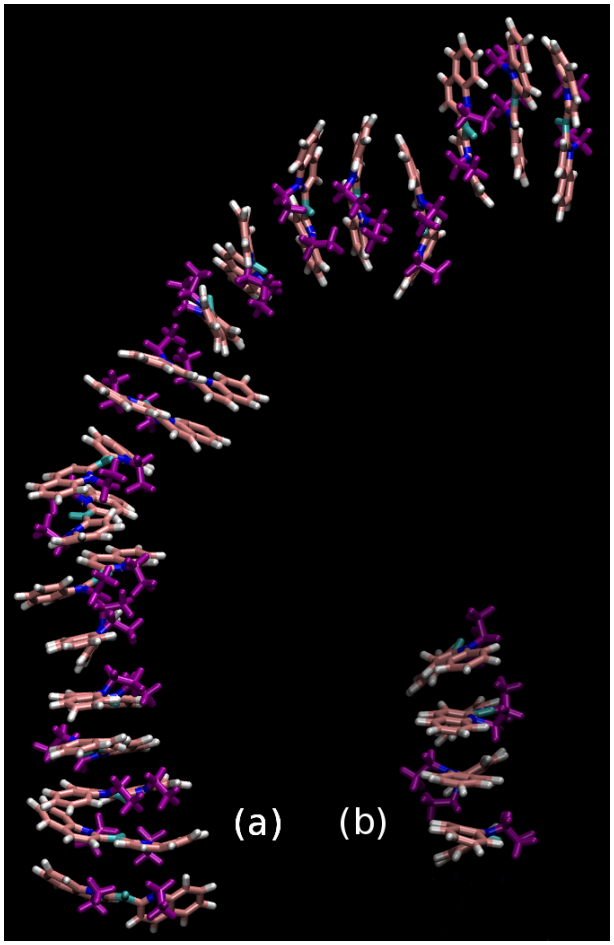

Figure 3: PIC oligomers with a pile-of-coins structure, formed in our MD simulations of the spontaneous aggregation process. (a) The largest self-aggregated structure that formed in our simulations, a pile of 19 PIC molecules. (b) A representative example of a PIC tetramer.

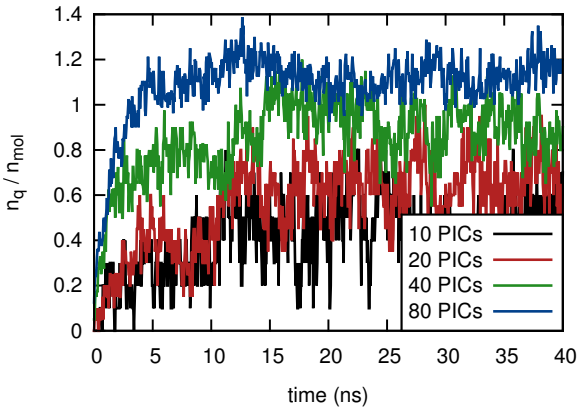

Figure 4: Characterization of the spontaneous aggregation process by the number of closely spaced quinoline rings n_q, corrected for the number of PIC molecules in the simulation box n_{mol}. Simulations were performed with 10, 20, 40 or 80 PIC molecules in the simulation box.

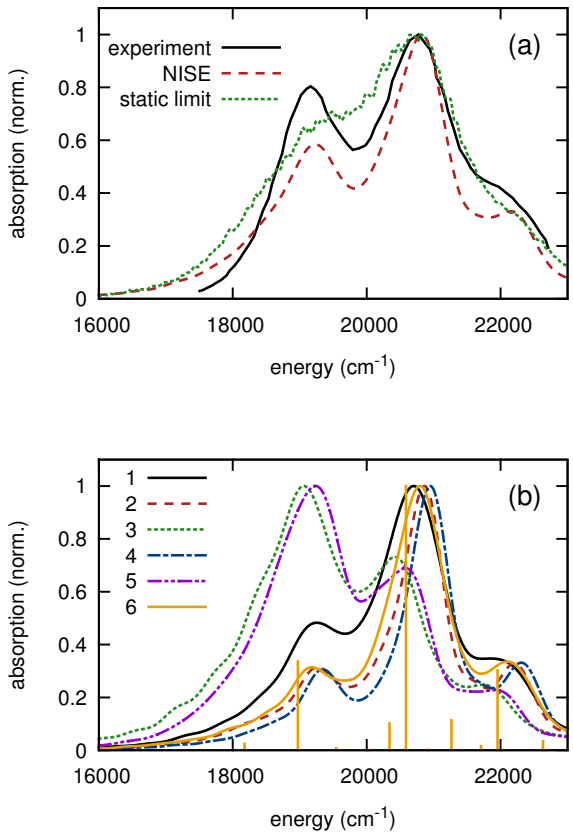

Figure 5: Absorption spectrum of the PIC dimer. (a) Obtained from experiment[20] (black solid curve) as well as simulated using the NISE method (red dashed curve) and the static limit (green dotted curve). Absorption maxima are normalized to unity. (b) Spectra of the six trajectories which were averaged over to obtain the NISE result shown in part (a). Trajectories 1, 2, and 3 were started from the configuration of dimer a at 0, 2.5, and 5 ns, respectively; trajectories 4, 5, and 6 used initial configurations from dimer b at the same times. The stick spectrum is the result of a simple dimer model, with parameters based on average values from trajectory 6. Note that the slight oscillations in the low-energy tail of some spectra are ringing artefacts, originating in the cutoff of the response funtion integral.[52]

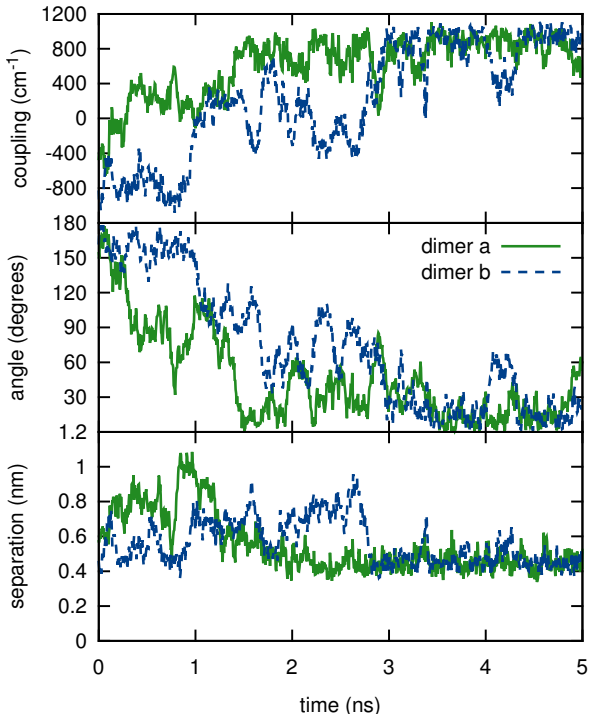

Figure 6: Characterization of the time evolution of two PIC dimers. (a) Excitonic coupling. (b) Angle between the transition dipoles. (c) Center-to-center distance.

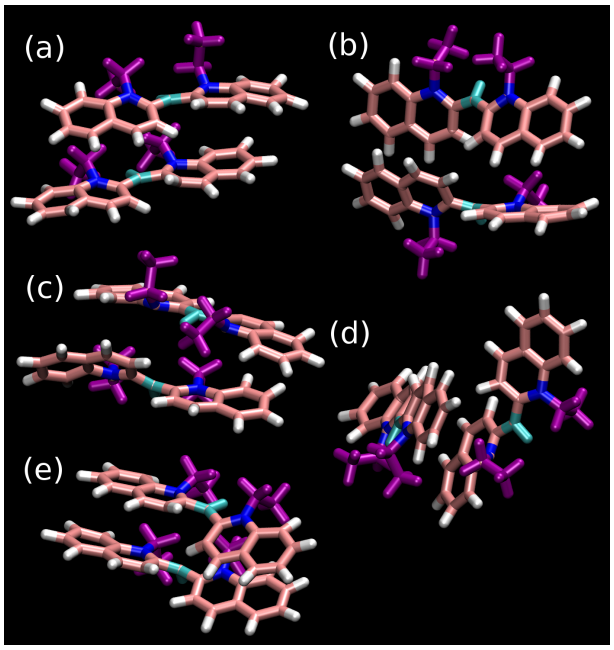

Figure 7: Several representative snapshots of dimer b from Figure 6. (a) 100 ps after the start of the production run: ethyl side groups of both PIC molecules are on the same side; (b) 200 ps: molecules are rotating with respect to each other; (c) 250 ps: after the rotation, ethyl side groups are located on opposite sides; (d) 2 ns: disorganized, unstable configuration of the dimer; (e) 5 ns: the dimer has stabilized and ethyl tails are back to the same side.

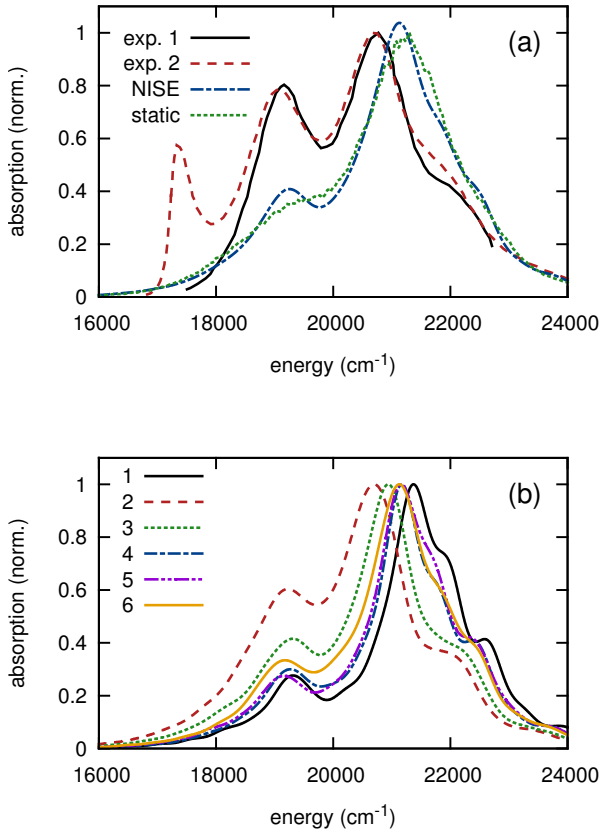

Figure 8: (a) Simulated absorption spectra of the PIC trimer, calculated in the static limit (green dots) and with the NISE method (blue dot-dashed curve), next to the dimer spectrum that was deduced from experiment by Kopainsky et al.[20] ("exp. 1", black solid curve), and the experimental spectrum that was measured at the onset of J-aggregation by von Berlepsch et al.[29] ("exp. 2", red dashed curve). (b) Spectra of the six trajectories which were averaged over to obtain the NISE result shown in part (a). Trajectories 1, 2, and 3 were started from the configuration of the first trimer at 0, 2.5, and 5 ns, respectively; trajectories 4, 5, and 6 used initial configurations from the second trimer at the same times.

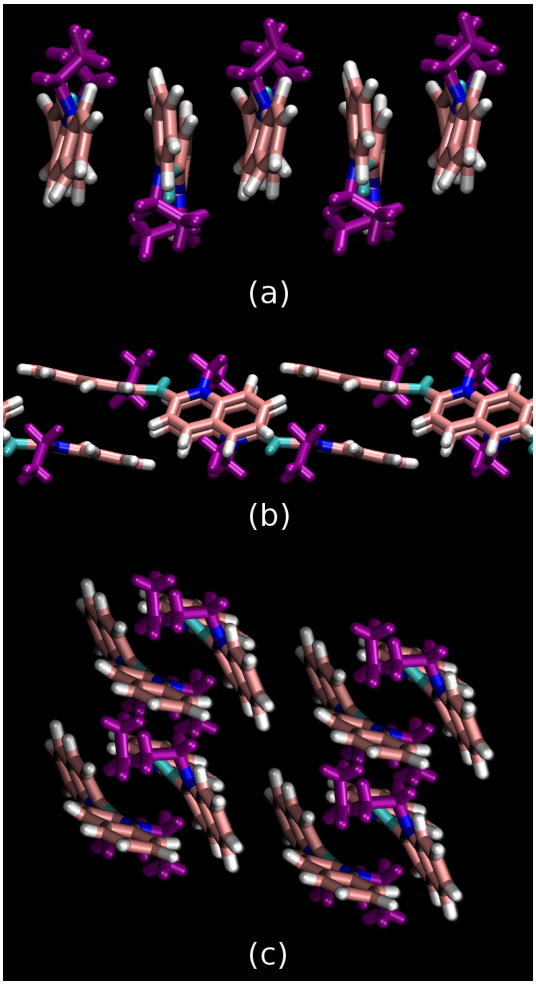

Figure 9: Three possible geometries of the PIC aggregate for which we tested the stability in MD simulations. (a) Pile-of-coins stack with the PIC molecules' ethyl side groups located on alternating sides of the aggregate. (b) Single strand, with quinoline rings π-π stacked in a parallel-displaced manner, taken from the experimentally determined crystal structure. Side view. (c) Four strands from the crystal structure. Top view.

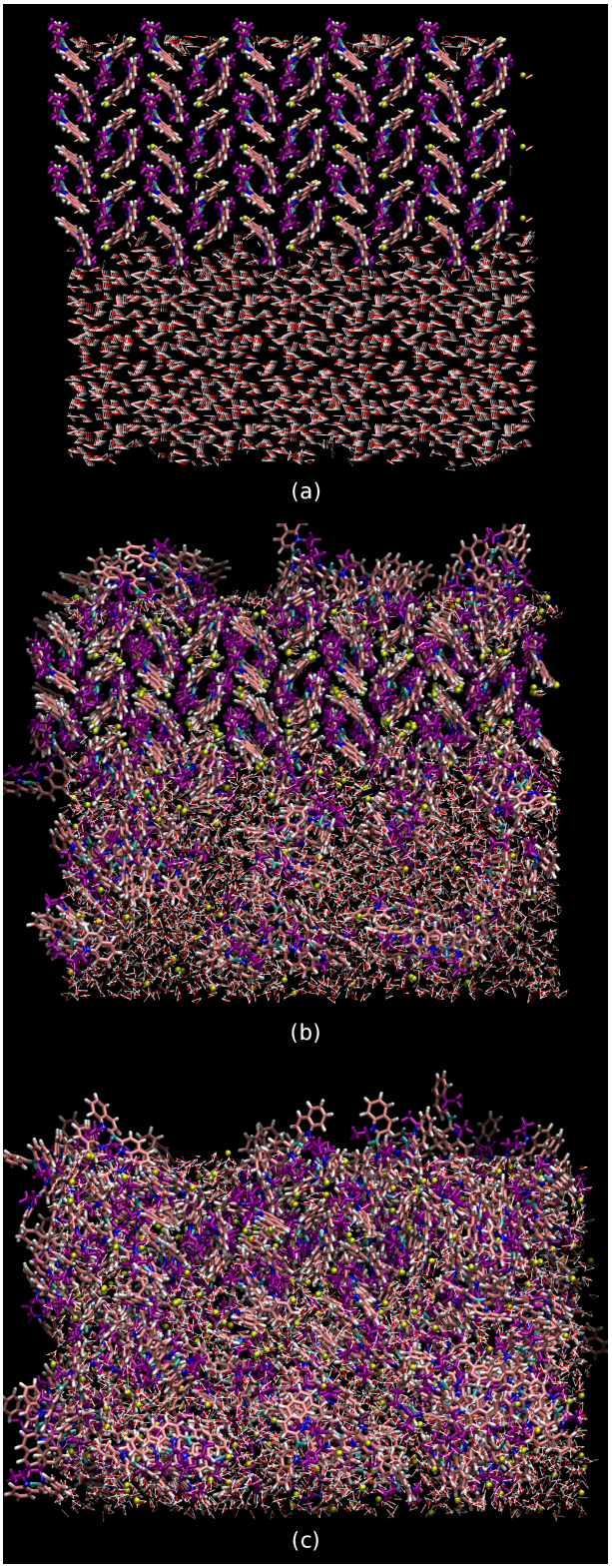

Figure 10: Snapshots from an MD simulation starting with half the simulation box occupied with PIC crystal, and the other half with water solvent. (a) Initial configuration. (b) After 10 ns. (c) After 20 ns.

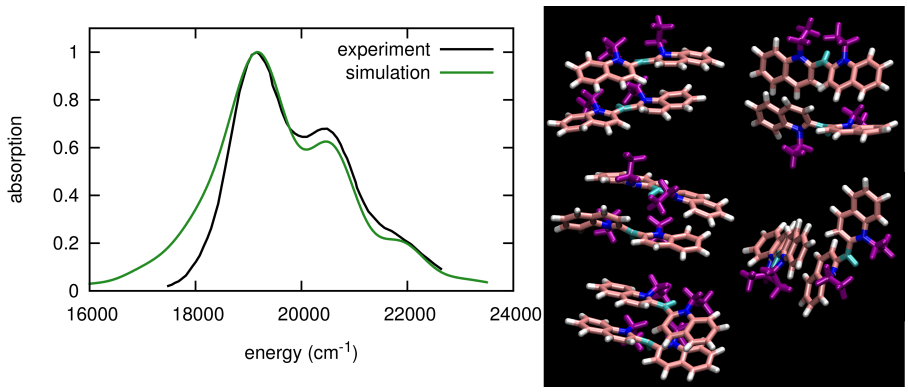

Figure 11: For table of contents only.